Journal of Sound and Vibration 347 (2015) 96–114

Contents lists available at ScienceDirect

Journal of Sound and Vibration

journal homepage: www.elsevier.com/locate/jsvi

Investigation of guided wave propagation and attenuation in pipe buried in sand

Eli Leinov *, Michael J.S. Lowe, Peter Cawley

NDE Group, Department of Mechanical Engineering, Imperial College London, London SW7 2AZ, UK

ARTICLE INFO

Article history:
Received 13 October 2014
Received in revised form
5 February 2015
Accepted 23 February 2015
Handling Editor: G. Degrande
Available online 16 March 2015

ABSTRACT

Long-range guided wave testing is a well-established method for detection of corrosion defects in pipelines. The method is currently used routinely for above ground pipelines in a variety of industries, e.g. petrochemical and energy. When the method is applied to pipes buried in soil, test ranges tend to be significantly compromised and unpredictable due to attenuation of the guided wave resulting from energy leakage into the embedding soil. The attenuation characteristics of guided wave propagation in an 8 in. pipe buried in sand are investigated using a laboratory full-scale experimental rig and model predictions. We report measurements of attenuation of the $T(0,1)$ and $L(0,2)$ guided wave modes over a range of sand conditions, including loose, compacted, mechanically compacted, water saturated and drained. Attenuation values are found to be in the range of 1.65–5.5 dB/m and 0.98–3.2 dB/m for the torsional and longitudinal modes, respectively, over the frequency of 11–34 kHz. The application of overburden pressure modifies the compaction of the sand and increases the attenuation. Mechanical compaction of the sand yields similar attenuation values to those obtained with applied overburden pressure. The attenuation decreases in the fully water-saturated sand, and increases in drained sand to values comparable with those obtained for compacted sand. Attenuation measurements are compared with Disperse software model predictions and confirm that the attenuation phenomenon in buried pipes is essentially governed by the bulk shear velocity in the sand. The attenuation behaviour of the torsional guided wave mode is found not to be captured by a uniform soil model; comparison with predictions obtained with the Disperse software suggest that this is likely to be due to a layer of sand adhering to the surface of the pipe.

1. Introduction

The inspection of pipelines by long-range Guided Wave Testing (GWT) has been routinely used for over a decade in a variety of applications in the petrochemical, power and nuclear industries [1–3]. The method employs ultrasonic signals guided by the inspected structure and offers the possibility of rapid screening over long lengths of pipework for the detection of corrosion and other defects. The common application of the method is to bare- or thinly epoxy-painted pipes. However, when the method is applied to pipes buried in soil, test ranges tend to be significantly reduced compared to bare pipes and unpredictable as the attenuation varies from case to case [4]. Buried pipes are generally tested by digging an

* Corresponding author. Tel.: +44 207 594 7227.
E-mail address: e.leinov@imperial.ac.uk (E. Leinov).

http://dx.doi.org/10.1016/j.jsv.2015.02.036
0022-460X/

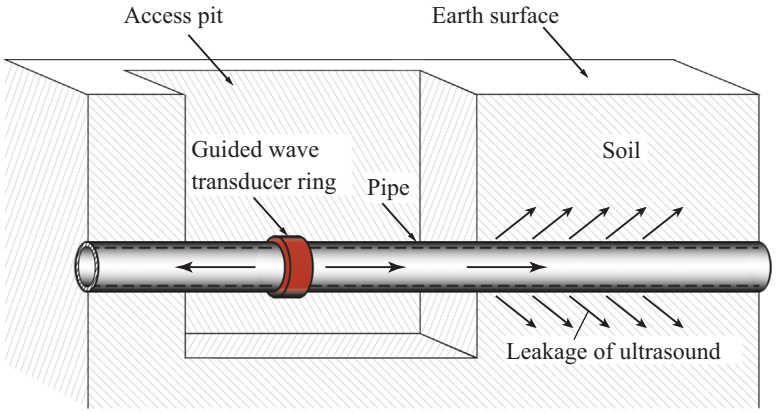

Fig. 1. Schematic of a pipe buried in soil. An access pit is excavated in order to perform guided wave inspection, where a guided wave transducer ring is attached to the pipe.

access pit to expose the pipe at the location where a transducer ring is to be attached as presented in Fig. 1. The testing scheme uses a pulse-echo arrangement from a single position on the inspected pipe. Waves are excited and received using a transducer ring comprising an array of dry-coupled piezoelectric elements equally spaced around the circumference of the pipe [5–7]. GWT typically requires frequencies below 100 kHz and employs the torsional ($T(0,1)$) or longitudinal ($L(0,2)$) modes. These modes are used since they are sensitive to cross-sectional loss at any location through the wall thickness or around the circumference, they are relatively easy to excite in their pure form and are generally non-dispersive over a wide frequency band [8–10]. The presence of soil in contact with the inspected pipe causes damping of the propagating guided wave modes since energy is leaking into the soil (Fig. 1), resulting in a dramatic reduction in test ranges. Moreover, the amount of leakage for a given mode depends on both the material properties of the pipe and the surrounding media, and in general is a function of frequency. The attenuation of these propagating modes may vary significantly from case to case since pipes are buried in different soil types and subjected to a variety of physical conditions, e.g. differences in water saturation of the soil along the pipe, soil compaction conditions and burial depths. The abundance of pipelines buried in the ground worldwide makes long-range GWT of these highly desirable and of high economic and environmental importance. Maximising the inspection range from a single access pit will minimise the number of access pits which have to be dug and reduce overall inspection costs significantly.

In the present study, we have conducted a comprehensive full-scale experimental investigation in order to characterise the damping of guided waves propagating in pipes buried in sand under a range of controlled physical conditions. Model predictions were used to reproduce the experimental results and to gain better understanding of the dominating physical mechanisms, with the aim of providing the scientific basis for the improved inspection of buried pipes.

The background on GWT in embedded cylinders is discussed in Section 2.1, the guided wave model is discussed in Section 2.2 and a review on soil acoustical properties is discussed in Section 2.3. The experimental apparatus and measurement method are described in Section 3. The experimental and model results are reported and discussed in Section 4 and the conclusion are provided in Section 5.

2. Background

2.1. Guided wave propagation in embedded cylinders

The propagation of acoustic waves along cylindrical structures has been studied extensively e.g. [11–15]. The use of ultrasonic GWT for the inspection of metallic structures is well established for several decades. For pipelines, GWT allows large pipe-lengths to be covered from a single transducer position, thus making it an economically attractive and time efficient technique. Many studies have focused on guided wave propagation in structures as means for detection and monitoring of defects and corrosion e.g. [1–10, 16–21].

However, although structures are commonly embedded or coated to provide insulation and corrosion protection in engineering applications, only a few studies has focused on these systems. In embedded or coated pipelines, the acoustic signal attenuates due to two mechanisms: damping by energy-absorbing materials of the waveguide system, and leakage of energy radiating out into the embedding material, resulting in a dramatic reduction of the test range. The rate of leakage depends on the material properties of both the pipe and the embedding material. For structures coated with materials having internal damping, e.g. bitumen, the attenuation is related to the amount of strain energy stored in the coating layer and is proportional to the frequency. As a consequence, there is a need for the understanding of the attenuation of guided waves propagating in pipes which are in direct contact with embedding or coating materials, in order to maximise the distance over which defects can be detected.

Progress in research into multi-layered systems [22,23] has produced descriptions of guided wave propagation in embedded and coated structures. Several studies have focused on leaky cylindrical waveguides, Pavlakovic et al. [24] studied circular steel bars embedded in cement grout, Beard and Lowe [25] studied rock bolts embedded in rock strata, and Beard et al. [26] studied reinforcing bars and anchor bolts embedded in concrete. Long et al. [27] studied guided wave propagation in iron pipes buried in soil and later steel bars embedded in soil [28]. Castaings and Lowe [29] studied arbitrary section waveguides embedded in solid media. Other studies have focused on attenuative coatings; Simonetti and Cawley [30] and Simonetti [31] derived the governing dispersion relation for guided wave propagation in elastic plates coated with viscoelastic materials. Barshinger and Rose [32] studied guided wave propagation in an elastic hollow cylinder coated with a viscoelastic material. Others have used the finite element method [33] and semi-analytic finite element method [34] to solve the governing dispersion relation in coated pipes, and more recently in coated pipes embedded in infinite soil media [35,36]. Kwun et al. [37] reported on attenuation measurements of the torsional guided wave in coal-tar-enamel-coated buried pipe. The scattering of the torsional and longitudinal guided waves from defects in coated pipes was discussed recently by Kirby et al. [38,39].

Some studies reported on the use of acoustic waves for leak detection from buried water pipes e.g. [40–42], however the acoustic frequency range used in this technique does not allow the detection of localised defects in pipes.

2.2. Guided wave modelling using Disperse software

The introduction of matrix techniques [43–46], initially developed to describe seismic wave propagation through layered rock strata, to multi-layered systems encountered in nondestructive inspection allowed a reliable prediction of guided wave propagation along structures. The Disperse modelling software [46–48] is based on partial wave theory and the global matrix technique. It provides rigorous predictions for guided wave propagation and dispersion in pipes, allows embedding the structure in solid materials, has layering capabilities, and is applicable over a range of frequencies. Dispersion curves are found iteratively in frequency, wavenumber and attenuation space.

In the model used in this study guided waves propagate along an infinite hollow cylinder embedded in an infinite soil medium. Continuity of displacements and stresses is imposed at the interface between the pipe and the soil. The dispersion of the guided wave is due to geometrical effects and leakage of energy to the embedding medium. The soil is assumed to behave as an elastic solid material since the guided waves introduce only small strain perturbations. The propagating mode displacements on the outer surface of the pipe excite bulk waves in the surrounding medium which radiate energy away from the pipe.

The Disperse software was used to predict the attenuation as a function of frequency for a variety of sand acoustic properties to match the different sand conditions covered in this study. Fig. 2 presents an example of dispersion curves of the zero-order modes for a Schedule-40, 8 in. pipe embedded in soil with representative acoustic properties. Fig. 2*a* shows the group velocities and the corresponding attenuation of the fundamental modes is presented in Fig. 2b. The $T(0,1)$ mode is non-dispersive for all frequencies, while the $L(0,2)$ mode is essentially non-dispersive over the ~20–100 kHz range. The attenuation values depend on the bulk velocities of the embedding medium and will vary for different acoustic properties of the soil.

2.3. Soil acoustic properties

The acoustic properties of the embedding soil dictate the amount of energy leakage from the waves guided along the pipe. Leakage arises when the phase velocity of the guided wave is larger than the bulk velocity in the embedding material.

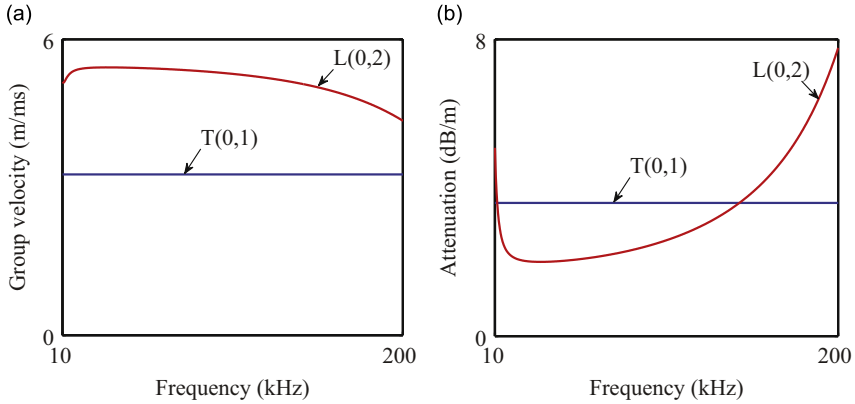

Fig. 2. Dispersion curves of the zero-order guided wave modes for 8 in. steel pipe (Schedule 40, 9 mm wall thickness, $\rho_{Steel}=7932\ kg\ m^{-3}$; $v_{L,Steel}=5960\ ms^{-1}$; $v_{S,Steel}=3260\ ms^{-1}$) embedded in sand ($\rho_{Sand}=1620\ kg\ m^{-3}$; $v_{L,Sand}=800\ ms^{-1}$; $v_{S,Sand}=105\ ms^{-1}$): (a) group velocity and (b) attenuation.

Table 1
Measured values of acoustic properties of sand reported in the literature.

Ref.	Medium	Condition	Density (kg m^{-3})	Method	Freq. (kHz)	Velocity		v_L attn. (dB m^{-1})	v_S attn. (dB m^{-1})
						v_L (ms^{-1})	v_S (ms^{-1})		
[28]	Sand	Saturated	N/A	Wave-guide	150	260–415	18–41	N/A	N/A
	Clay	Moist	1900–1950			900–1900	4–80		
	Alnwick soil	Moist	2100			350	72		
[51]	Sand (beach)	Dry	N/A	Seismic	N/A	150–300	100–190	N/A	N/A
[52]	Sand (beach)	N/A	1600	Seismic	0.15–0.6	150	75	N/A	N/A
[53]	Silt loam	Moist	620–950	Transmission	10–26	N/A	N/A	1–26	N/A
	Sand	Moist	1050–1370		10–26	N/A	N/A	3–13	N/A
	Mud	Saturated	N/A		10–35	N/A	N/A	25–74	N/A
[54]	Fine Sand	Varied saturation	1650	Transmission	30	90–220	N/A	N/A	N/A
	Silt loam	Varied saturation	1250			80–190	N/A	N/A	N/A
[55]	Sand	Dry	N/A	Transmission	0.5–16	120–240	N/A	1.3–10	N/A
[56]	Sand	Varied saturation	1805.4	Transmission	4	150–350	80–210	N/A	N/A
[57]	Various	Varied saturation	790–1620	Transmission	2–6	86–260	N/A	0.24–5.76	N/A
[58]	Silica sand	Saturated	2047	Transmission	4–20	N/A	140–240	N/A	7.5–35
[59]	Silica sands	Saturated	2011–2030	Transmission	4–20	N/A	115–140	N/A	5.5–35
[60]	Sand	Moist[a]	N/A	Bender element	N/A	N/A	120–200	N/A	N/A
[61]	Silica	Sat.[a]	N/A	Bender element	N/A	N/A	50–300	N/A	N/A
	Kaolinite						70–220		
[66]	Sand, various	Dry[a]	N/A	Transmission	100	550–650	290–380	Q-factor	N/A
		Sat.[a]	N/A			1750–1950	310–390		
[67]	Sand (beach)	Saturated	N/A	Transmission	1000	2633–2962	190–435	Q-factor	N/A
[68]	Sand	Dry[a]	N/A	Transmission	200	350–750	180–360	N/A	N/A
		Sat.[a]	N/A			1500–2000	180–360		

[a] Medium is pressure loaded. Values presented here correspond to the lowest value of applied pressure loading reported in the reference.

If the opposite situation occurs, the guided wave becomes non-leaky. Wave velocities and attenuation in soils depend on the wave parameters, e.g. frequency, wavelength and mode of propagation, and are influenced by a range of geophysical properties, e.g. grain density and diameter, compaction, porosity, degree of saturation and bulk and shear moduli.

Generally, the velocity of the longitudinal wave is a function of the bulk and shear stiffnesses of the soil, whilst the velocity of the shear wave depends only on the shear stiffness. The shear stiffness of the soil is the shear stiffness of its skeleton and is much smaller than the bulk stiffness of the soil particles material [49]. The stiffness of the skeleton depends on inter-particle forces, i.e. skeletal and local contact between particles, and on the particle material. In fully saturated soils the bulk stiffness depends on the porosity, the bulk stiffness of the fluid and the bulk stiffness of the soil particles material, and it is not sensitive to the stiffness of the skeleton. The presence of air dramatically reduces the bulk stiffness of the fluid and the longitudinal velocity becomes a function of the skeleton alone [49].

A large amount of work has been published in the geophysics and the geotechnical engineering literature on the measurement of porous and particulate media material properties, mostly in the framework of exploration seismology, earthquake engineering and structural stability. Velocities of the longitudinal and shear waves are typically measured with a pulse transmission technique in which an energy source is used to produce acoustic waves that travel through the medium to receivers. Seismic surveying methods are inherently designed to characterise deep formations, hence very few studies have reported on in-situ velocity measurements in near-surface unconsolidated soils (e.g. [50–52]).

Laboratory measurement techniques of soil acoustic properties include direct transmission (e.g. [53–59]), the use of bender elements (e.g. [60–62]), resonance column (e.g. [63]) and free vibrations (e.g. [64]). Fratta and Santamarina [65] determined velocities and attenuation in the laboratory with transmission of guided waves from a steel rod through a soil sample to accelerometers using a multimode waveguide. Long et al. [28] used a waveguide technique to measure the attenuation characteristics of the longitudinal mode that propagates in a steel bar embedded in near-surface soils, from which the acoustic properties of the soils were inferred both in the laboratory and in-situ. The influences of depth and water saturation on wave propagation in soils are studied experimentally using triaxial cells, allowing confinement of soil samples and application of stress (e.g. [66–68]). Because of transducer–soil coupling problems and complexity of data interpretation, laboratory measurements at atmospheric and low pressures are hard to conduct and few are in the literature.

The measured velocity and attenuation values for unconsolidated soils reported in the literature are summarised in Table 1. For unconsolidated sands with various saturation values, the shear wave velocity is reported in the range of 18–300 ms^{-1} [28,51,52,56,58–60,61] and the longitudinal wave velocity in the range of 80–415 ms^{-1} [28,51,52,54–57]. The shear and longitudinal wave velocities increase with pressure loading. Typically, the lowest applied pressure in a triaxial soil-cell is 0.1 MPa. Wave velocities reported at this pressure value for dry sand are in the range of 180–380 ms^{-1} for the shear velocity and 310–750 ms^{-1} for the longitudinal velocity [66,68], and for saturated sand are in the range of 180–435 ms^{-1} for the shear velocity and 1500–2962 ms^{-1} for the longitudinal velocity [66–68]. Indeed, the range of wave velocities reflects the complex nature of wave propagation in soils.

3. Experimental method

A full scale laboratory apparatus was designed to allow systematic and well-controlled experimental conditions in order to characterise the effect of the different physical parameters on the attenuation of ultrasound in a pipe buried in soil.

3.1. Experimental apparatus

The buried pipe experimental apparatus consisted of a 5.67-m long, 8 in. carbon steel pipe (schedule-40, 9 mm wall thickness) embedded for 3-m of its length in a rectangular container of 0.76 m × 0.76 m inner cross-section (Fig. 3a, b). The container walls were made from 40 mm-thick plywood plates and reinforced with a combination of rectangular section steel beams (MkII Soldiers, Harsco Infrastructure) on each wall in order to support the load from the soil; the beams on opposite walls were connected with tie-bars. The container was fitted with an inner tank-liner (Greenseal EPDM, Sealeco) to allow water saturation of the soil. The pipe was fitted to the container at the entry and exit positions through circular apertures in the tank-liner. The apertures had a smaller diameter than that of the pipe in order to allow the liner material to be stretched for ~20 mm along the pipe axis and provide sealing to the container. Circular openings were made in the corresponding wooden faces of the container, forming a 20 mm gap around the pipe from the opening edge, in order to allow the pipe to settle in the sand without making contact with the openings in the wooden faces. A rectangular inflatable air-bladder (3 m × 0.76 m × 0.1 m, Polyurethane fabric, Chiorino) was fitted between the soil surface and the container covering plate in order to allow the application of different pressure loads on the soil corresponding to different depth conditions. The air-bladder was connected in line with an air compressor (Clarke), needle valve regulator and air pressure gauge (RS). A soil pressure gauge (KDC-PA 200 kPa, TML) was used at the centre of the bottom plate in order to monitor the pressure within the body of the sand. The pressure gauge has a circular sensing diameter of 100 mm and was calibrated using an independent load cell. Fig. 3c–e presents photographs of the operating apparatus.

Ultrasonic guided waves were generated in the pipe using commercial transducer rings (Guided Ultrasonics Ltd.) and signals were transmitted and collected using the Wavemaker G4 instrument (Guided Ultrasonics Ltd.). The transducer ring consists of dry-coupled piezoelectric transducer elements which are clamped to the pipe surface using an air-inflatable sleeve. It has the capability to excite either $L(0,2)$ or $T(0,1)$ modes at different central frequencies, depending on the

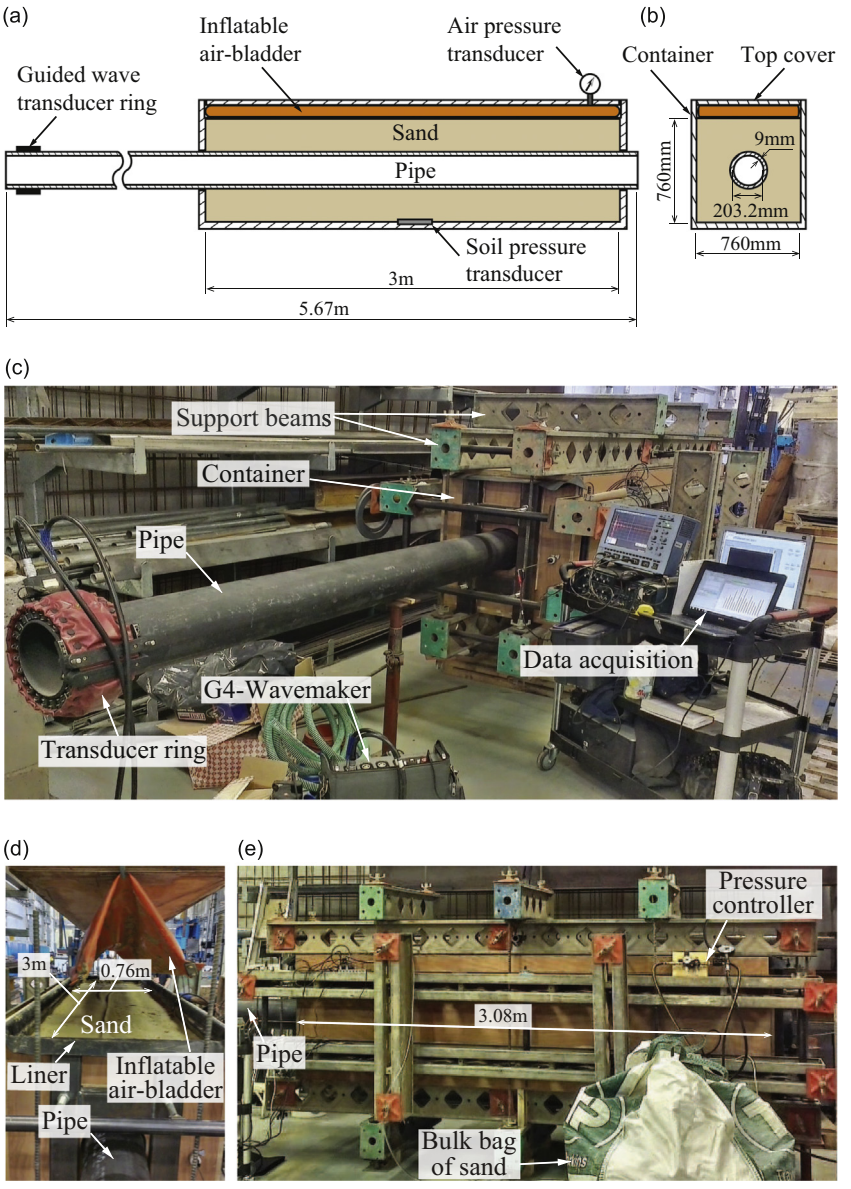

Fig. 3. Full-scale experimental apparatus: (a) side view drawing, (b) front view drawing, (c) photograph of the operating apparatus with the pipe embedded in sand in the container, the transducer ring attached to the pipe and the data acquisition system, (d) front view photograph with the sand, tank-liner and inflatable air-bladder evident, and (e) side view photograph with the pressure control system.

orientation of the transducers comprising the ring and their spacing. Two independent transducer rings were used for the torsional and longitudinal modes in order to avoid the need to rotate transducers between experiments; they were attached in turn along the exposed length of the pipe.

The soil selected as the working medium was well graded clean sand [69] (sand grain density of 2600 kg m^{-3}). This type of sand may be used as a structural backfill material and complies with standard practice for pipeline installation. The particle size distribution of the sand is presented in Fig. 4 and was determined using a laboratory sieving test (Electromechanical vibratory sieve column shaker, Controls). The sand particles were found to be finer than 1.25 mm, with the majority (73 percent) not finer than 0.6 mm. None of the particles was found to be finer than 0.075 mm.

3.2. Experimental set-up

Five different sets of experiments were conducted in order to characterise the influence of the sand physical conditions on the attenuation of the guided ultrasonic waves in the pipe. The sand conditions covered in this study are: dry loose, dry compacted, dry mechanically compacted, water saturated and drained. The sand bulk densities associated with the different

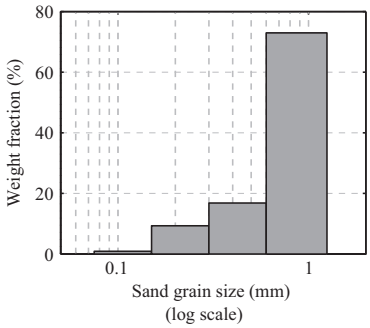

Fig. 4. Grain size distribution for the sand used in this study.

Table 2
Conditions of sand and bulk density values covered in this study.

Case	Condition	Sand bulk density (kg m^{-3})
Loose	Nominally dry	1455
Compacted	Nominally dry	1620
Mechanically compacted	Nominally dry	1660
Water saturated	Saturated	1895
Drained	Partially wet	1724

cases are presented in Table 2. The bulk densities were determined from measurement of the net weight of sand or sand and water used to fill the container and the volume it occupied in the container. The procedures used to generate the experimental conditions are detailed in the following sub-sections.

3.2.1. *Loose and compacted sand*

Dry loose sand was poured into the empty container from bulk bags which were held above the container using a crane. Sand was filled and distributed evenly without application of any compaction effort up to ca. 30 mm above the lowest point of the container pipe entry and exit apertures; once this point was reached, the pipe was introduced into the container. The pipe was positioned with one end of the container adjacent to one end of the pipe while the remaining section of the pipe was exposed to air. The pipe was allowed to settle on top of the sand prior to fixing two support posts for the rest of the filling process to make sure the pipe was not making contact with the container walls. Sand was poured further in the same manner as described above to backfill the container up to a height of 0.76 m (Fig. 3b). The support posts were then released, allowing the pipe to settle in the sand. The air-bladder was introduced above the sand top surface once the sand was levelled (Fig. 3a and d) and the container was sealed from the top by its covering plate. Once the air-bladder was connected to the air-compressor pressure could be applied; overburden loading pressures of up to 1 bar, an equivalent to ca. 6 m depth of dry sand with uniform density, were applied on the sand in order to modify its compaction and to simulate different depths of the buried pipe. The air-bladder was inflated slowly and once a desired pressure value was achieved it was kept constant. The bulk density of the compacted sand was estimated from measurement of the height of sand in the container after completing the tests for this case.

3.2.2. *Mechanically compacted sand*

The mechanically compacted sand tests were set-up using a mechanically vibrating plate (0.3 m $\times$ 0.496 m, 50 kg operating weight, 97 Hz vibrating frequency, WP1030A, Wacker Neuson) and a manual backfill rammer (0.1 m $\times$ 0.1 m). Dry loose sand was poured to the empty container from bulk bags and distributed in the container in layers of 120 mm in height at a time. Each layer was compacted using the vibrating plate, operated over the same period of 15 min to ensure equal compaction for each layer. The pipe was introduced to the container once the sand fill reached up to ca. 20 mm above the lowest point of the container pipe entry and exit openings. The pipe was positioned in the same way as in the previous case and support posts were used to fix the pipe position for the rest of the filling process. Sand layers were then introduced and compacted using the manual rammer, in order not to damage the pipe, until the pipe was completely covered with sand. Sand was layered and compacted further with the vibrating plate up to a height of 0.76 m. The support posts were then released to allow the pipe to settle in the sand and the air-bladder was introduced between the sand surface and the container covering plate and overburden loading pressures were applied.

3.2.3. Saturated and drained sand

The saturated sand tests were set-up by initially introducing the pipe into the container at a vertical position just above the centre of the openings using two support posts, one at 1.25 m from the exposed end of the pipe and the other at the end of the pipe, adjacent to the container exit. The posts were fitted with wooden supports in order to minimise reflections from the support (see [70]). The container was filled with water up to height of 0.175 m. Dry loose sand was poured slowly into the water from bulk bags in the same fashion as previous cases. Water was added as the height of the sand increased until the height of the saturated sand reached 0.76 m. A poker-vibrator was used in order to evacuate residual trapped air from the saturated sand. The support posts were readjusted after allowing the pipe to settle to the middle of the entry and exit openings. The air-bladder was introduced between the saturated sand surface and the container covering plate to allow overburden pressure loading. Once the saturated sand case tests finished, water was pumped out from wells that were excavated to the bottom of the container near its walls. Water drained from the sand to the wells for four days before ceasing. The water collected from the drainage of the sand allowed the determination of density of the drained sand in the container.

In all of the cases, guided wave experiments were conducted after the sand bottom pressure stabilised.

3.3. Measurement technique

Both $L(0,2)$ and $T(0,1)$ guided waves were excited and recorded in separate independent tests for all of the conditions covered using two different transducer rings. Two different transducer ring locations were used, at the exposed pipe end and near the entrance to the container, to confirm repeatability, for each condition and for both modes. Received raw signals obtained from the transducer rings were converted to the frequency domain via Fourier transform; a Hilbert envelope was applied to the signals in order to determine the amplitudes of the reflections peaks. Two different central frequencies, 16.5 kHz and 23.5 kHz, were used for each mode to allow some overlap of the frequencies in the range covered.

The attenuation characteristic was obtained from the ratio of the signal amplitudes measured from the pipe end reflections:

$$\alpha = -\frac{20\log_{10}(A_1/A_0)}{2L} \tag{3.1}$$

where L is the length of the pipe embedded in sand, A_0 is the reference reflection amplitude and A_1 is the measurement amplitude. When the transducer ring is attached at the free end of the pipe, both reference reflection and measurement signals are received echoes from the far end beyond the buried section, while when the ring is attached adjacent to the entrance to the buried section the reference reflection signal is received echo from the free end and the measurement signal is received echo from the pipe-end beyond the buried section. In both cases the propagation distance in the buried section between the reference and measurement reflections is $2L$. The attenuation in the exposed section of the pipe is due to material damping and not leakage of energy as in the embedded section. The attenuation of both modes was found to be less than 0.1 dB m^{-1} in reference tests performed on the bare pipe in air; hence the attenuation of the modes in the pipe section exposed to air is considered to be negligible.

To interpret the data, a series of dispersion curves was produced, using the Disperse modelling software [46–48], for a steel pipe embedded in an infinite layer of sand with a variety of possible values of acoustic parameters. The acoustic properties of the sand were extracted from the best fit to the experiments. The use of two different modes in two independent tests for each experimental condition allows verification of the model predictions with a high degree of confidence.

We have originally tried implementing the ultrasonic waveguide ('dipstick') technique [28] in order to obtain an independent measurement of the acoustic properties of the sand (see [71]). This technique required measurement of the

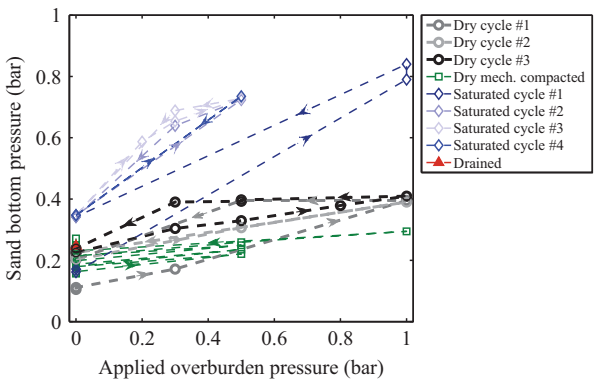

Fig. 5. Applied overburden pressure histories for loose and compacted sand, mechanically compacted sand, saturated sand and drained sand. Arrows indicate the chronology of loading and unloading of the sand.

attenuation characteristics of the longitudinal mode that propagates along an embedded rod, from which the acoustic properties of the surrounding medium are inferred. However, we have found only limited success with this technique due to poor coupling between the dipstick and the surrounding sand for some of the cases, particularly when it was dry; this method was therefore abandoned.

4. Results

4.1. Pressure histories

Overburden pressure was applied on the sand in order to modify its compaction and to simulate in the laboratory load conditions a pipe would be subjected to at approximately 6 m depth below the earth surface. The load applied on a buried pipe by the soil used for backfill can be estimated by the weight of the soil above the pipe. Overburden pressure was applied in all the experimental sets except for the drained sand case. The resulting pressure at the bottom of the sand in the container provides an indication of the compaction of the sand. The pressure histories for the different cases are presented in Fig. 5. The sand bottom pressure is shown as a function of applied overburden pressure. Values presented correspond to stabilised sand bottom pressure following the application of constant overburden pressure using the air-bladder. Typically, applied pressure values were kept constant for a minimum period of one hour.

Beginning with the dry loose sand case, the initial sand bottom pressure was 0.11 bar and three pressure cycles were applied in steps up to overburden pressure of 1 bar. The first cycle, for example, consisted of the application of 0.3 bar followed by 1 bar before unloading to 0.5 bar, then to 0.3 bar and unloading the overburden pressure completely. The sand bottom pressure responded markedly to increasing the load on the sand, while the unloading resulted in a retarded decrease of the pressure. The bottom pressure has reached an average of 0.4 (± 0.01) bar at 1 bar applied overburden pressure, over the three loading cycles. The bottom pressure at rest (no applied overburden pressure) increased with the number of loading cycles, from 0.2 bar after the first cycle to 0.24 bar after the third cycle, indicating that the sand compaction increased. The density has increased from an initial value of 1455 kg m^{-3} in the loose sand to 1620 kg m^{-3} for the final compacted state. The loading and unloading of the overburden pressure on the sand exhibit hysteretic behaviour. Identical values of applied overburden pressure resulted in different values of sand bottom pressure, depending both on the path, i.e. loading or unloading, and on the chronology, i.e. cycle number of loading or unloading.

The initial sand bottom pressure in the mechanically compacted case was approximately 0.16 bar and the bulk density was determined to be 1660 kg m^{-3}. Four pressure cycles were applied in this case. The first three cycles consisted of application of 0.5 bar followed by unloading completely, and the fourth cycle consisted of application of 0.5 bar followed by 1 bar before unloading completely. The maximum pressure reached in this case was ca. 0.29 bar. The sand bottom pressure at rest increased from 0.23 bar after the unloading of the last cycle to a final value of 0.27 bar. The bottom pressure behaviour in these loading cycles is very similar since the sand was pre-compacted and no further compaction could be achieved. Pressure values reported here are in good agreement with values found in the literature for earth pressures in retaining wall configurations (e.g. [72–73]).

The bottom pressure in the saturated sand case was initially ca. 0.17 bar and the bulk density was determined to be 1895 kg m^{-3}. Four pressure cycles were applied for this case. The initial cycle consisted of application of 1 bar, resulting in 0.79 bar at the bottom of the sand, and keeping the overburden pressure for 14 h to allow any trapped air in the saturated sand to diffuse towards the sand surface and to allow the sand to compact, resulting in an increase of the bottom pressure to 0.84 bar, before unloading completely. The following three cycles consisted of application of 0.5 bar, resulting in identical bottom pressure of 0.73 bar, followed by unloading, resulting in bottom pressure of 0.35 bar at rest. The hysteretic behaviour

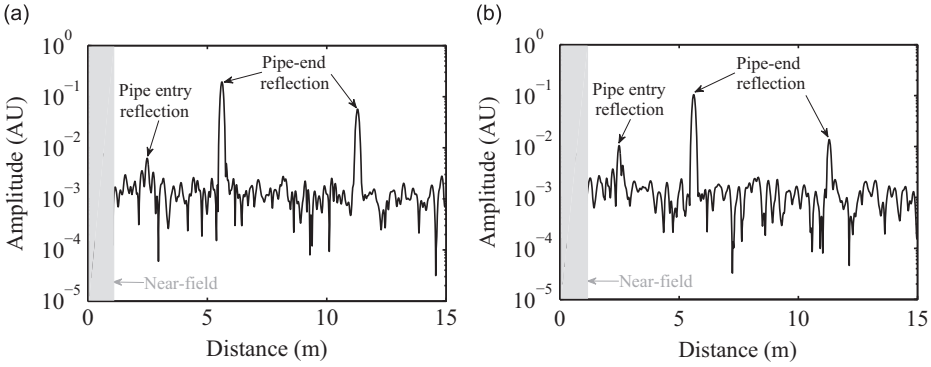

Fig. 6. Typical experimental results from the buried pipe: amplitudes (in arbitrary units) as a function of distance from the transducer ring, located adjacent to one of the pipe ends, using $T(0,1)$ mode at central frequency of 23.5 kHz. Grey shaded rectangle is the near field: (a) loose sand and (b) compacted sand (1 bar applied pressure).

of the sand was noticed in the saturated case as well; however, following the first cycle it appears that the sand has compacted to its maximum capacity since the last three cycles have reached identical values of bottom pressure under loading and at rest. No loading cycles were applied in the drained sand case. The bottom pressure stabilised at ca. 0.25 bar once the drainage of water stopped and the bulk density was estimated to be 1724 kg m^{-3}. The bulk density of the drained sand was larger than the compacted sand and smaller than the saturated sand, indicating residual water remained in the sand.

4.2. Guided wave testing and Disperse simulations

Typical experimental results obtained from two different guided wave tests performed on a pipe buried in loose sand and in compacted sand (overburden pressure of 1 bar applied) are presented in Fig. 6a, b. The mode of excitation was $T(0,1)$ at a central frequency of 23.5 kHz. The results are displayed as amplitude of the Hilbert envelope of the recorded signal on a logarithmic scale as a function of distance from the transducer ring position. The ring position in both cases is at the free end of the pipe. Two pipe-end reflections are clearly evident from which the attenuation measurement is inferred using Eq. (1). Also evident are reflections from the location of the pipe entry to the container. The entry reflection was larger in the compacted sand case (Fig. 6b) than in the loose sand case (Fig. 6a). It should be noted that the entry reflection introduces an error in the attenuation measurements. An estimate of the error could be obtained using the energy balance equation [74]:

$$R^2+T^2=1 \tag{4.1}$$

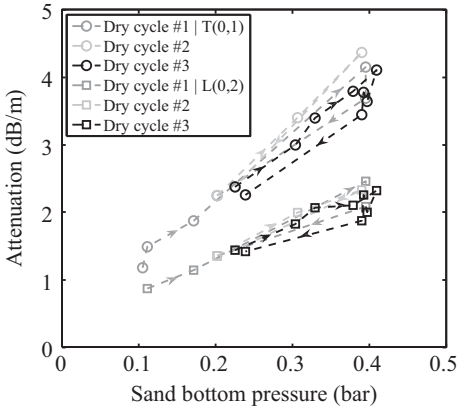

Fig. 7. Attenuation measurements of the $T(0,1)$ (circles) and $L(0,2)$ (squares) modes as a function of sand bottom pressure for three overburden pressure cycles applied on the dry sand at central frequency of 23.5 kHz.

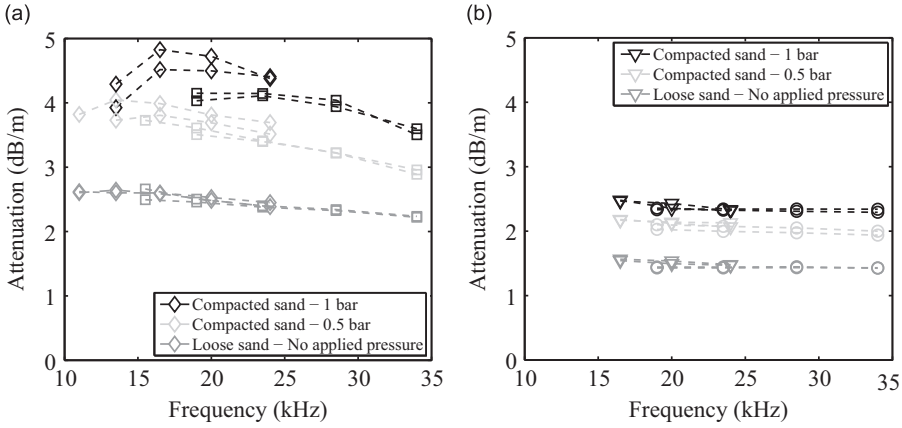

Fig. 8. Attenuation measurements as a function of frequency in the dry sand case for three different overburden pressures, 1 bar (black), 0.5 bar (light grey) and no applied pressure (dark grey), for (a) $T(0,1)$ mode and (b) $L(0,2)$ mode. Diamonds and triangles correspond to 16.5 kHz central frequency and squares and circles to 23.5 kHz central frequency.

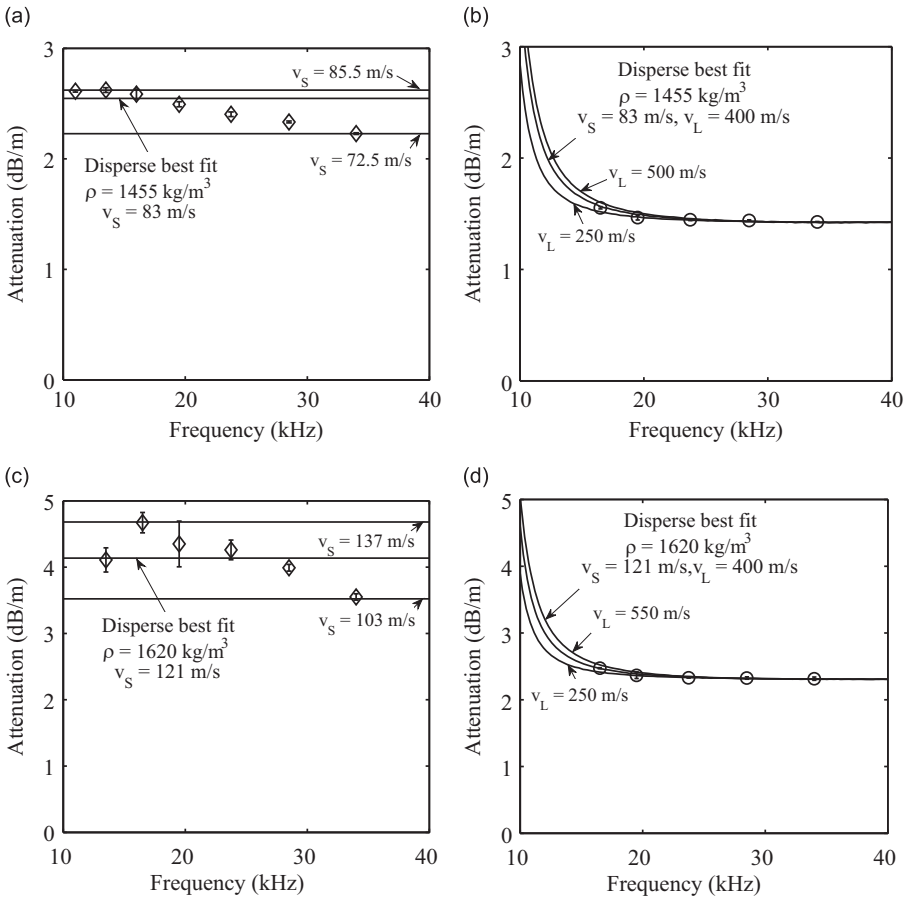

Fig. 9. Attenuation measurements as a function of frequency and Disperse simulation fits (solid lines) in the loose sand, of (a) $T(0,1)$ mode (diamonds) and (b) $L(0,2)$ mode (circles), and in the compacted sand, of (c) $T(0,1)$ mode (diamonds) and (d) $L(0,2)$ mode (circles).

In the results presented here the entry reflection was found to be less than 15 percent of the pipe end reflection in the compacted sand cases and less than 8 percent in all other cases. This corresponds to a maximum attenuation error of 0.1 dB m^{-1}. The measurement could have been corrected to compensate for the entry reflection error and the resulting overestimation of the attenuation; however, the maximum error is small compared to the measured attenuation and it was not always possible to measure the entry reflection accurately, hence we present measurements as they were obtained.

4.2.1. Loose and compacted sand

Attenuation measurements of the $T(0,1)$ and $L(0,2)$ modes at a central frequency of 23.5 kHz as a function of sand bottom pressure for the three loading cycles applied on the loose and compacted sand are presented in Fig. 7. The attenuation of the torsional mode is found to be larger than that of the longitudinal mode and the attenuation of both modes is roughly proportional to sand bottom pressure with some evidence of hysteresis as the pressure is loaded and unloaded.

Fig. 8 presents the attenuation of the $T(0,1)$ and $L(0,2)$ modes in the frequency domain for the dry loose sand (no applied pressure) and dry compacted sand under 0.5 bar and 1 bar applied overburden pressure. Two sets of measurements, obtained from different ring positions along the free length of the pipe, are presented for the two central frequencies used in each case. The application of overburden pressure modifies the compaction of the sand and significantly increases the attenuation of both modes. The attenuation of the torsional mode (Fig. 8a) in the three cases presented is larger than the attenuation of the longitudinal mode (Fig. 8*b*). The torsional mode exhibits some frequency dependence, mostly in the compacted sand case (1 bar applied pressure).

Comparing results obtained from different ring positions at the same central frequency shows a relatively larger variation for the torsional mode in the compacted sand case compared to the loose sand case. A maximum variation of 7 percent was found at a frequency of 16.5 kHz in the compacted sand, whilst the variation for the same frequency in the loose sand was found to be less than 1 percent. The same trend was found for results obtained from different central frequencies in the overlapping range of frequencies. A maximum variation of 14 percent at a frequency of 20 kHz was found for the compacted

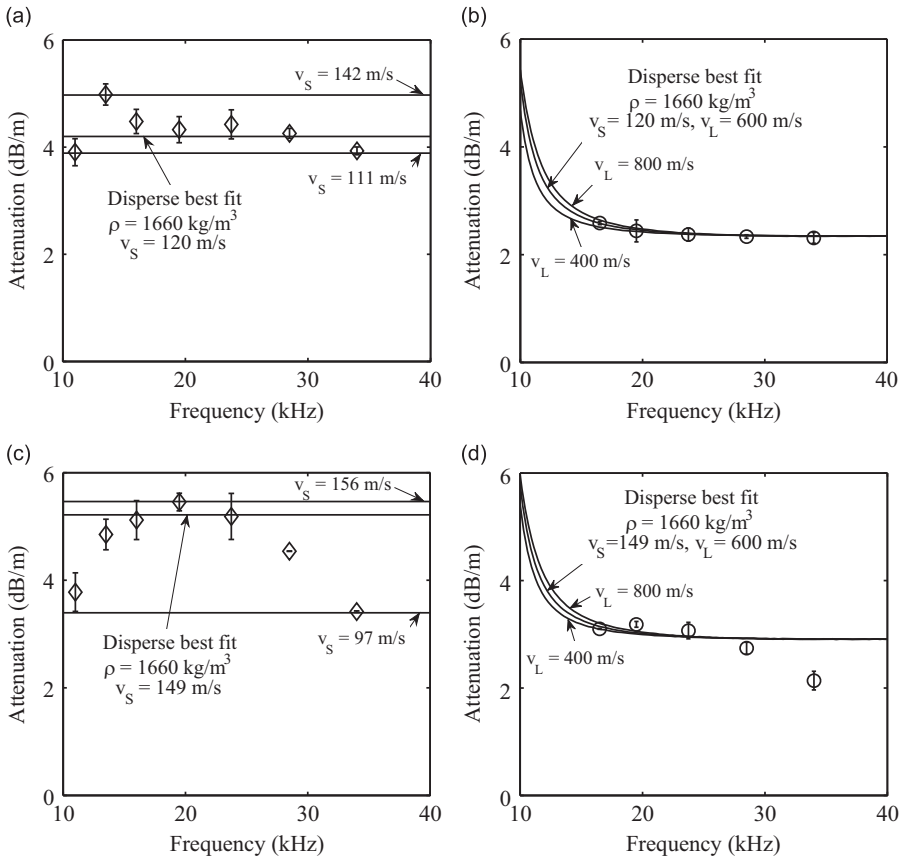

Fig. 10. Attenuation measurements as a function of frequency and Disperse simulation fits (solid lines) in the mechanically compacted sand: (a) *T*(0,1) mode (diamonds), (b) *L*(0,2) mode (circles) just after compaction, and (c) *T*(0,1) mode (diamonds), (d) *L*(0,2) mode (circles) three months later.

sand case, whilst the variation for the same frequency in the loose sand was less than 2 percent. Smaller variation between results was found for the longitudinal mode, with less than 3 percent for different ring positions and less than 5 percent between different central frequencies.

The Disperse software was used to predict the attenuation as a function of frequency for a variety of sand acoustic velocities and the estimated density (Table 2). Fig. 9 presents Disperse simulation fits to the attenuation as a function of frequency measured in each mode in the loose and compacted sand experiments. The measured attenuation in a particular sand condition at a particular frequency is the average of the values obtained from the different ring positions and excitation centre frequencies; error bars represent the variation between measurements at a certain frequency. The lower and upper average torsional mode attenuation values were fitted to give the lowest and highest values of shear velocities (lighter solid lines in Figs. 9a and c) in the range of frequencies covered. The best fit curve is determined from the fit to the longitudinal mode attenuation (Fig. 9b and d); a single value of shear velocity is found to match the longitudinal mode attenuation at higher frequencies. The extracted best fit values of the shear velocity are 83 ms^{-1} and 121 ms^{-1} for the loose and compacted sand cases, respectively. The longitudinal attenuation is relatively insensitive to the sand longitudinal velocity so this cannot be estimated accurately. However, the range of values for both shear and longitudinal velocities is within the range of the measurements reported in the literature shown in Table 1.

4.2.2. Mechanically compacted sand

We now focus on two sets of experiments performed on the mechanically compacted sand. The first set of measurements was undertaken just after completing the compaction process using the mechanical compacting plate and the second three months later. Fig. 10 presents average attenuation measurements obtained for both torsional and longitudinal modes and Disperse simulation fits. The maximum variation between measurements obtained at the same central frequency with different torsional ring position was found to be 9 percent, and a maximum variation of 8 percent between measurements obtained at different central frequencies. The measured attenuation just after compaction and Disperse simulation fits (Fig. 10a, b) are similar to the attenuation in the compacted sand case previously discussed (Fig. 9c, d). This, as well as comparable bulk density values (Table 2), indicates that equivalent compaction conditions have been achieved. Fig. 10c, d

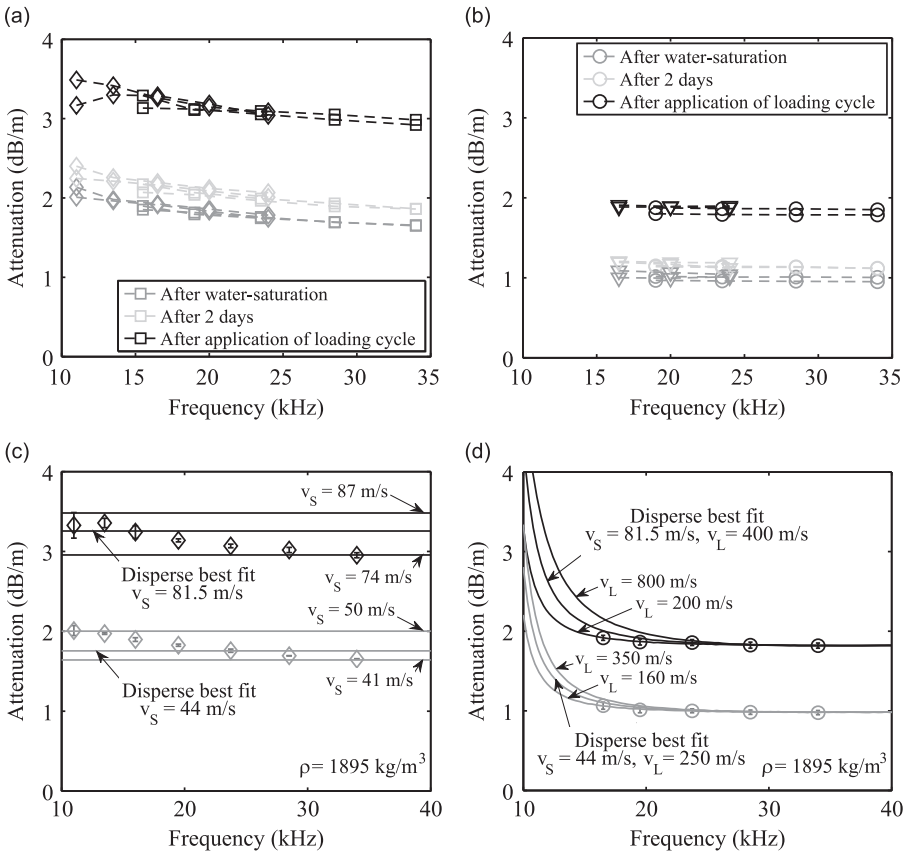

Fig. 11. Saturated sand tests. (a) $T(0,1)$ mode and (b) $L(0,2)$ mode attenuation measurements as a function of frequency at three times, immediately after saturating the sand, two days later and after the application of a pressure cycle (see Fig. 5) (diamonds and triangles correspond to 16.5 kHz central frequency and squares and circles to 23.5 kHz central frequency); (c) $T(0,1)$ mode (diamonds) and (d) $L(0,2)$ mode (circles) average attenuation measurements and Disperse simulation fits (solid lines) immediately after saturation (grey) and after the application of a pressure cycle (black).

shows the corresponding results for the second set. The attenuation of both modes reached larger values in the later set of tests and the frequency dependence of both modes attenuation has substantially increased. The longitudinal mode attenuation measurements for both cases are smaller than those for the torsional mode. The frequency dependence of the attenuation will be discussed in detail in Section 4.3.

4.2.3. Saturated and drained sand

Fig. 11 presents the measurements of the torsional and longitudinal modes attenuation for the saturated sand and the corresponding Disperse simulation fits. Fig. 11a, b shows measurements performed at three different times, immediately after completing the saturation of the sand, after two days, and after the application of the first loading cycle (see Fig. 5). The attenuation of the modes immediately after saturation is smaller compared to values measured for previous cases. The corresponding shear velocity values are as well small compared to values found for other cases, probably because water does not support shear and the sand was not well coupled to the pipe. The longitudinal mode attenuation values are smaller than the torsional mode for all three sets shown for the saturated sand. The increase of the attenuation after two days is attributed to settling effects in the saturated sand. The application of a pressure cycle resulted in further increase of attenuation for both modes by approximately a factor of two, due to modified compaction of the sand. Under applied load it is easier for the sand grains to overcome grain-to-grain friction and move in a water saturated environment than in the dry case; moreover, the sand may also compact if trapped air is present. The attenuation of the torsional mode exhibits slight frequency dependence for all three cases. Disperse simulation fits to average attenuation measurements from the first and last experimental sets are presented in Fig. 11c, d. After the application of the pressure loading, the corresponding shear velocity values increase as the sand was more compacted; however, the values are lower than those obtained for the dry compacted sand cases.

Fig. 12 presents attenuation measurements along with Disperse simulation fits for the drained sand case. Fig. 12a, b shows three experimental sets corresponding to three times, after completing the four day long water-drainage, 14 and 39

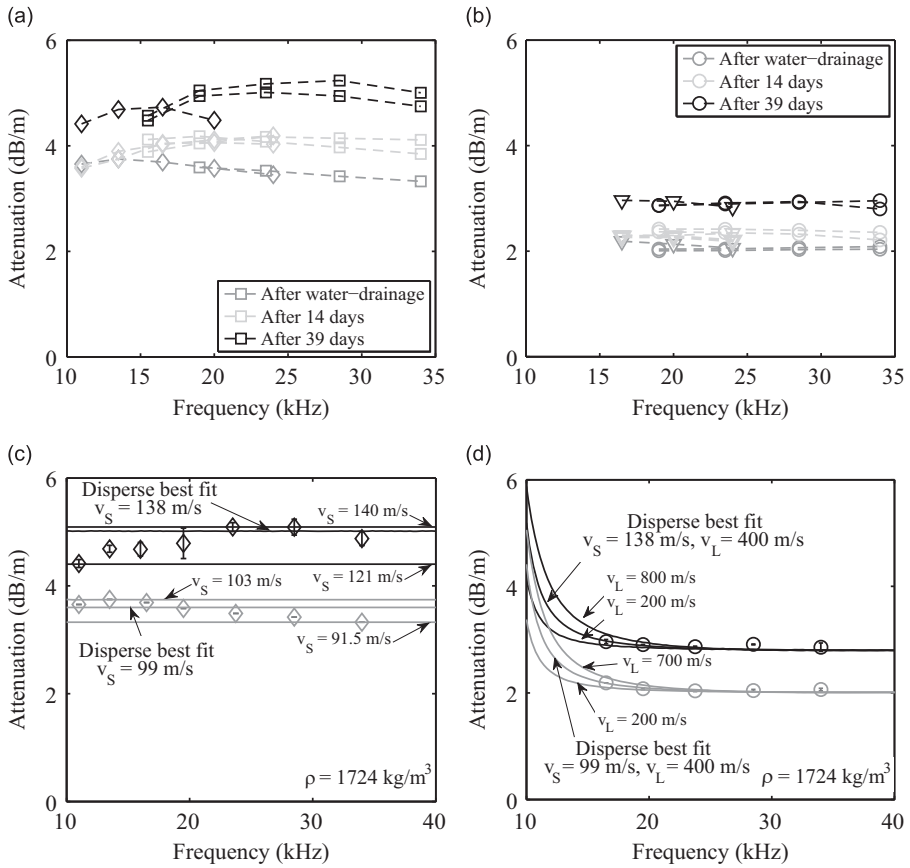

Fig. 12. Drained sand tests: (a) $T(0,1)$ mode and (b) $L(0,2)$ mode attenuation measurements as a function of frequency at three times, after water-drainage stopped, 14 days later and 39 days later (diamonds and triangles correspond to 16.5 kHz central frequency and squares and circles to 23.5 kHz central frequency); (c) $T(0,1)$ mode (diamonds) and (d) $L(0,2)$ mode (circles) average attenuation measurements and Disperse simulation fits (solid lines) after water-drainage stopped (grey) and 39 days later (black).

days later. The attenuation of both modes is higher than in the saturated sand case and it is found to increase with time due to consolidation of the sand. Similarly to previous cases, the longitudinal mode attenuation values are smaller than those of the torsional mode for all three sets. Some frequency dependence can be seen in the torsional mode cases while the longitudinal mode measurements are almost frequency independent over the range measured. Simulation fits to average attenuation measurements from the first and third experimental sets are presented in Fig. 12c, d. The attenuation values and the corresponding shear velocity values obtained for the drained sand case are comparable to values obtained for the dry compacted sand cases.

4.3. Disperse two-layer model

The frequency dependence of the torsional mode attenuation was investigated next. Initially, shear wave velocity dispersion, such as that observed in [58,59] was incorporated into Disperse uniform-infinite sand layer model; however, it yielded only increasing attenuation with frequency. Exposing the pipe subsequent to each of the experimental cases revealed a crust of sand adhering to the pipe surface. The frequency dependence of the torsional mode attenuation was particularly strong in the mechanically compacted sand case; hence we have investigated whether a layer of sand adjacent to the pipe with slightly different properties compared to the bulk embedding material could explain the observed frequency dependence. In the modified model used in Disperse, the pipe is embedded in a medium consisting of a thin layer of sand adjacent to the pipe and a surrounding second infinite-layer of sand, as shown in Fig. 13a. The thin layer of sand has a finite thickness and slightly different shear velocity than the shear velocity of the second, infinite layer. The thickness of the first layer was set to vary in the range of 1–2 times the mean sand particle diameter (see Fig. 4). Higher shear velocity in the thin sand-layer could be caused by different contact conditions experienced by the sand grains that are in contact with the pipe compared to those that are in contact only with their neighbouring sand grains; it

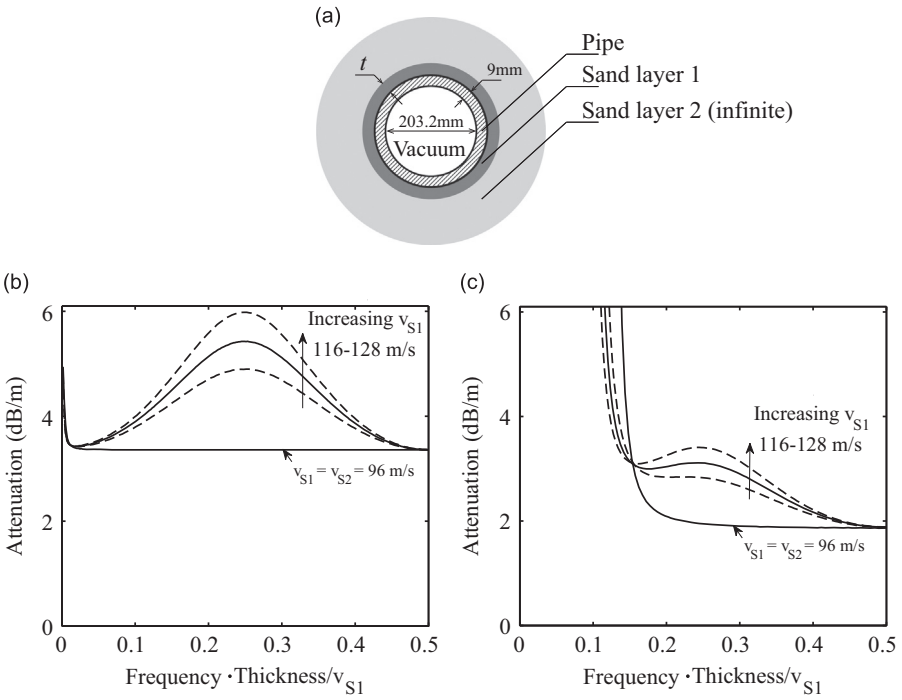

Fig. 13. Two-layer model: (a) schematic diagram of the physical system comprising a pipe and two layers of sand. The first layer of thickness t and the second layer is infinite; (b) $T(0,1)$-mode attenuation, and (c) $L(0,2)$-mode attenuation, as a function of the non-dimensional frequency (the product of frequency-thickness over the shear velocity in the first layer) simulated with Disperse for values corresponding to the mechanically compacted sand case. Different curves correspond to varied values of shear velocity in the first layer (v_{S1} =96–128 ms^{-1}) whilst keeping the shear velocity of the second layer constant (v_{S2} =96 ms^{-1}). The density is equal for both layers ($\rho_{S1}=\rho_{S2}=1660$ kg m^{-3}).

could also be caused by the onset of corrosion generating corrosion-products that may mix with the sand and also make the sand adhere to the pipe.

It was found that the leakage of ultrasound in the two-layer model is governed by the shear velocities of the two layers and their difference. Fig. 13b, c shows the attenuation of both modes as a function of the product of the frequency-first-layer thickness, normalised by the shear velocity in the first layer (non-dimensional frequency). The density and shear velocity for the outer, infinite layer correspond to the mechanically compacted sand of Fig. 10c, d, i.e. density of 1660 kg m^{-3} for both layers and shear-velocity value of 96 ms^{-1} for the second infinite layer, estimated based on the single-uniform-model simulation fit. The two-layer model reproduces the single uniform layer model when the shear velocities in both layers are equal. Increasing the shear velocity of the first layer results in an increase of the torsional mode attenuation with a maximum when the layer thickness is a quarter wavelength. The maximum value obtained is a function of the shear velocity of the thin layer; as the thickness of the layer is changed, the absolute frequency at which the peak occur shifts, since it always occurs at a non-dimensional frequency of 0.25.

The embedding layer properties were adjusted to fit the experimental results from the different cases by first determining the inner and outer layer shear velocities that give the measured maximum and minimum values of torsional mode attenuation (the minimum occurs at the highest frequencies measured while the peak occurs as described above). The inner layer thickness is then adjusted so that the maximum attenuation occurs at the correct frequency. Fig. 14 shows the two-layer model simulation fits to measured attenuation of the modes for two sets of measurements where relatively strong frequency dependence was observed, namely, the mechanically compacted sand (Fig. 10c, d), and the drained sand (Fig. 12c, d). The attenuation behaviour for both torsional and longitudinal modes is captured excellently with the two-layer simulation best fit for both sets of experiments. Most of the measurement values are found to lie within the bounds representing a 5 percent variation of the shear velocity of the thin layer of sand. The best fit thickness of the first layer in the two-layer model was found to be 1.5 mm for the mechanically compacted case and 1.2 mm for the drained sand case; both values are of the order of the sand grain size (Fig. 4), supporting the hypothesis that the effect is caused by a layer of sand adhering to the pipe. Similar simulation fits were obtained for the rest of the cases covered in this study. The best fit parameter values used for all cases are summarised in Table 3, along with values obtained for the uniform embedding layer model.

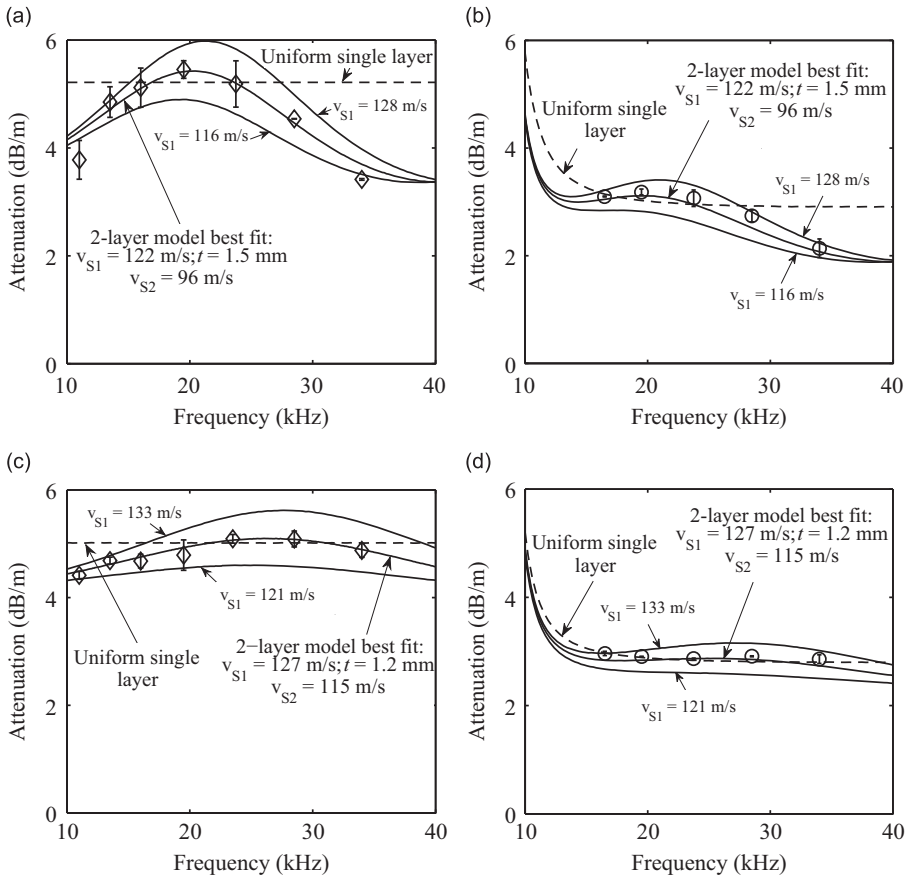

Fig. 14. Two-layer model fit to attenuation measurements as a function of frequency. (a) $T(0,1)$- and (b) $L(0,2)$-modes for the latter case of the mechanically compacted sand ($\rho_{S1}=\rho_{S2}=1660$ kg m^{-3}); and (c) $T(0,1)$- and (d) $L(0,2)$-modes for the latter case of the drained sand ($\rho_{S1}=\rho_{S2}=1724$ kg m^{-3}). The two-layer best fit and bounds representing 5% variation of the shear velocity in the first thin layer are indicated. Also shown is the uniform-single-layer model best fit (dotted lines).

Table 3
Disperse simulations fitting parameters using uniform- and two-layer models.

	Uniform (infinite) layer model		Two-layer model			
			1st (thin) layer[a]		2nd (infinite) layer	
Case	ρ (kg m^{-3})	v_S (ms^{-1})	v_{S1} (ms^{-1})	Thickness (mm)	ρ_2 (kg m^{-3})	v_{S2} (ms^{-1})
Compacted	1620	121 (103–137)	118	1.6	1620	102
Mech. compacted I[b]	1660	120 (111–142)	118	1.5	1660	110
Mech. compacted II[c]	1660	149 (97–156)	122	1.5	1660	96
Saturated I[b]	1895	44 (41–50)	44	0.7	1895	41
Saturated II[d]	1895	81.5 (74–87)	77	1.2	1895	74
Drained I[b]	1724	99 (91.5–103)	97	1.5	1724	91
Drained II[e]	1724	138 (121–140)	127	1.2	1724	115

[a] Density of the thin layer equal to the value used for the single-layer model.
[b] Immediately after process complete.
[c] Three months after compaction.
[d] After application of loading cycle.
[e] After 39 days.

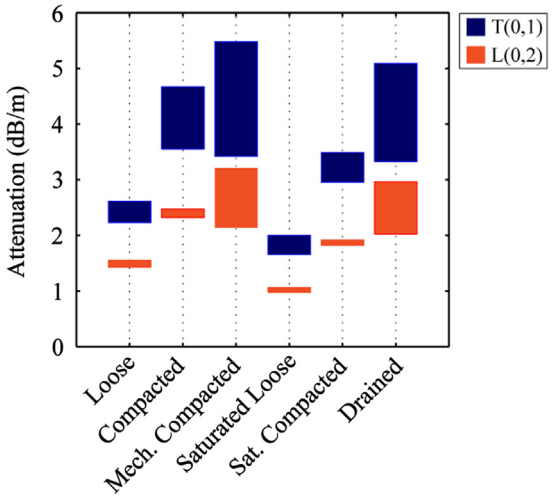

Fig. 15. Measured $T(0,1)$ (blue) and $L(0,2)$ (red) modes attenuation range of values over frequency band of 11–34 kHz for all sand conditions covered in this study.

5. Conclusions

Full-scale laboratory tests of guided waves propagation in an 8 in. pipe (Schedule-40, 9 mm wall thickness) buried in sand have been conducted over a range of sand conditions, including loose and compacted, mechanically compacted, under applied overburden pressure, water saturated and drained. Guided waves were excited in the pipe using two transducer rings and attenuation was measured for $T(0,1)$ and $L(0,2)$ modes independently over the frequency range of 11–34 kHz. A summary of the measured attenuation for both modes is presented in Fig. 15. Attenuation values were found to be in the range of 1.65–5.5 dB/m and 0.98–3.2 dB/m for the torsional and longitudinal modes, respectively. The application of overburden pressure on the sand modifies its compaction and increases the attenuation of the guided waves. Mechanical compaction of the sand yields similar attenuation values to those obtained with applied overburden pressure. The attenuation decreases in the fully water-saturated sand, while it increases in drained sand to values comparable with those obtained for the compacted sand. The $L(0,2)$ mode exhibits lower attenuation values than the $T(0,1)$ mode for the physical conditions of sand covered in this study.

The comparison of the measured attenuation with model predictions confirms that the attenuation in both the longitudinal and torsional modes is essentially governed by the shear velocity in the sand. A constant shear velocity in the embedding medium yields frequency-independent torsional mode attenuation; however, in some cases clear evidence of frequency dependence was observed. It was shown that this can be explained by the presence of a thin layer adjacent to the pipe with a slightly higher shear velocity than the bulk sand; further evidence for the presence of such a layer was found when the pipe was removed from the rig and a thin crust adhering to the pipe was observed.

The high values of attenuation and the large variability with sand condition show why GWT test ranges are greatly reduced in buried pipes and are very variable. Pipe-damage detection capabilities are determined by the signal to coherent noise ratio (see e.g. [1]). From the attenuation values it is possible to deduce expected test ranges that will allow reflections from defects to travel back to the transducer ring. The understanding of the fundamental physical parameters governing the leakage of ultrasound from buried pipes gained in this study could provide avenues for the design of buried pipe coating that will allow test ranges to be increased.

Acknowledgements

The authors gratefully acknowledge support from the UK Engineering and Physical Sciences Research Council (EPSRC) in this work, under research Grant EP/J01284X/1 and the UK Research Centre in Nondestructive Evaluation (RCNDE). This work was carried out in collaboration with BP Exploration Operating Company Ltd, EDF Energy, EDF R&D and Shell Global Solutions International BV.

The authors would like to thank the four reviewers for their constructive comments.

E.L. would like to thank Mr. Leslie Clark and the Structures Laboratory staff at the Department of Civil Engineering, Imperial College London, for the excellent technical support.

References

[1] D.N. Alleyne, B. Pavlakovic, M.J.S. Lowe, P. Cawley, Rapid long-range inspection of chemical plant pipework using guided waves, *Insight*1354-2575 43 (2) (2001) 93–101.
[2] P. Mudge, Field application of the Teletest long-range ultrasonic testing technique, *Insight* 43 (2001) 74–77.
[3] M. Sheard, A. McNulty, Field experience of using long-range ultrasonic testing, *Insight* 43 (2001) 79–83.
[4] V.M. Nunez Ledesma, E. Perez Baruch, A. Demma, Lowe MJS., Guided wave testing of an immersed gas pipeline, *Materials Evaluation* 67 (2) (2009) 102–115. ISS**N** 0025-5327.
[5] D.N. Alleyne, P. Cawley, The excitation of Lamb wAaves in pipes using dry-coupled piezoelectric transducers, *Journal of Nondestructive Evaluation* 15 (1) (1996) 11–20, http://dx.doi.org/10.1007/BF00733822.
[6] D.N. Alleyne, M.J.S. Lowe, P. Cawley, The reflection of guided waves from circumferential notches in pipes, *Journal of Applied Mechanics* 65 (3) (1998) 635–641, http://dx.doi.org/10.1115/1.2789105.
[7] M.J.S. Lowe, D.N. Alleyne, P. Cawley, Defect detection in pipes using guided waves, *Ultrasonics* 36 (1998) 147–154, http://dx.doi.org/10.1016/S0041-624X(97)00038-3.
[8] P. Cawley, Practical long range guided wave inspection – managing complexity AIP Conference Proceedings, Vol. 657, D.O. Thompson, D.E. Chimenti (Eds.), *Review of Progress in Quantitative Nondestructive Evaluation*, Vol. 22, AIP, New York2003, pp. 22–37, http://dx.doi.org/10.1063/1.1570116.
[9] A. Demma, P. Cawley, M.J.S. Lowe, A.G. Roosenbrand, B. Pavlakovic, The reflection of guided waves from notches in pipes: a guide to interpreting corrosion measurements, *NDT & E International* 37 (2004) 167–180, http://dx.doi.org/10.1016/j.ndteint.2003.09.004.
[10] D.N. Alleyne, T. Vogt, P. Cawley, The choice of torsional or longitudinal excitation in guided wave pipe inspection, *Insight* 51 (7) (2009) 373–377, http://dx.doi.org/10.1784/insi.2009.51.7.373.
[11] D.C. Gazis, Three-dimensional investigation of the propagation of waves in hollow circular cylinders. I: analytical foundation, *Journal of the Acoustical Society of America* 31 (1959) 568–573, http://dx.doi.org/10.1121/1.1907753.
[12] D.C. Gazis, Three-dimensional investigation of the propagation of waves in hollow circular cylinders. II: numerical results, *Journal of the Acoustical Society of America* 31 (1959) 573–578, http://dx.doi.org/10.1121/1.1907754.
[13] J. Zemanek, I. Rudnick, Attenuation and dispersion of elastic waves in cylindrical bar, *Journal of the Acoustical Society of America* 33 (1961) 1283–1288, http://dx.doi.org/10.1121/1.1908417.
[14] J. Zemanek, An experimental and theoretical investigation of elastic wave propagation in a cylinder, *Journal of the Acoustical Society of America* 51 (1972) 265–283, http://dx.doi.org/10.1121/1.1912838.
[15] B.A. Auld, *Acoustic Fields and Waves in Solids*, 2nd edition, Krieger, Florida. ISBN: 0-89874-782-1, 1990.
[16] W. Mohr, P. Holler, On inspection of thin-walled tubes for transverse and longitudinal flaws by guided ultrasonic waves, *IEEE Transactions on Ultrasonics Ferroelectrics and Frequency Control* 23 (5) (1976) 369–374, http://dx.doi.org/10.1109/T-SU.1976.30893.
[17] M.G. Silk, K.F. Bainton, The propagation in metal tubing of ultrasonic wave modes equivalent to Lamb waves, *Ultrasonics* 17 (1) (1979) 11–19, http://dx.doi.org/10.1016/0041-624X(79)90006-4.
[18] D.N. Alleyne, P. Cawley, The interaction of Lamb waves with defects, *IEEE Transactions on Ultrasonics Ferroelectrics and Frequency Control* 39 (3) (1992) 381–397, http://dx.doi.org/10.1109/58.143172.
[19] J.J. Ditri, Utilization of guided elastic waves for the characterization of circumferential cracks in hollow cylinders, *Journal of the Acoustical Society of America* 96 (1994) 3769–3775, http://dx.doi.org/10.1121/1.410565.
[20] M.J.S. Lowe, D.N. Alleyne, P. Cawley, Defect detection in pipes using guided waves, *Ultrasonics* 36 (1998) 147–154, http://dx.doi.org/10.1016/S0041-624X(97)00038-3.
[21] J.L. Rose, *Ultrasonic Guided Waves in Solid Media*, Cambridge University Press, Cambridge, 2014. ISBN: 978-1-107-04895-9.
[22] A.H. Nayfeh, The propagation of horizontally polarized shear waves in multilayered anisotropic media, *Journal of the Acoustical Society of America* 86 (5) (1989) 2007–2012, http://dx.doi.org/10.1121/1.398580.
[23] A.H. Nayfeh, P.B. Nagy, General study of axisymmetric waves in layered anisotropic fibers and their composites, *Journal of the Acoustical Society of America* 99 (2) (1996) 931–941, http://dx.doi.org/10.1121/1.414621.
[24] B.N. Pavlakovic, M.J.S. Lowe, P. Cawley, High-frequency low-loss ultrasonic modes in imbedded bars, *Journal of Applied Mechanics* 68 (2001) 67–75, http://dx.doi.org/10.1115/1.1347995.
[25] M.D. Beard, M.J.S. Lowe, Non-destructive testing of rock bolts using guided ultrasonic waves, *International Journal of Rock Mechanics and Mining* 40 (2003) 527–536, http://dx.doi.org/10.1016/S1365-1609(03)00027-3.
[26] M.D. Beard, M.J.S. Lowe, P. Cawley, Ultrasonic guided waves for inspection of grouted tendons and bolts, *Journal of Materials in Civil Engineering* 15 (3) (2003) 212–218, http://dx.doi.org/10.1061/(ASCE)0899-1561(2003)15:3(212).
[27] R. Long, M.J.S. Lowe, P. Cawley, Attenuation characteristics of the fundamental modes that propagate in buried iron water pipes, *Ultrasonics* 41 (2003) 509–519, http://dx.doi.org/10.1016/S0041-624X(03)00166-5.
[28] R. Long, T. Vogt, M.J.S. Lowe, P. Cawley, Measurement of acoustic properties of near-surface soils using an ultrasonic waveguide, *Geophysics* 69 (2) (2003) 460–465, http://dx.doi.org/10.1190/1.1707065.
[29] M. Castaings, M.J.S. Lowe, Finite element model for waves guided along solid systems of arbitrary section coupled to infinite solid media, *Journal of the Acoustical Society of America* 123 (2) (2008) 696–708, http://dx.doi.org/10.1121/1.2821973.
[30] F. Simonetti, P. Cawley, On the nature of shear horizontal wave propagation in elastic plates coated with viscoelastic materials, *Proceedings of the Royal Society of London: Series A* 460 (2004) 2197–2221, http://dx.doi.org/10.1098/rspa.2004.1284.
[31] F. Simonetti, Lamb waves propagation in elastic plates coated with viscoelastic materials, *Journal of the Acoustical Society of America* 115 (5) (2004) 2041–2053, http://dx.doi.org/10.1121/1.1695011.
[32] J.N. Barshinger, J.L. Rose, Guided wave propagation in elastic hollow cylinder coated with a viscoelastic material, *IEEE Transactions on Ultrasonics Ferroelectrics and Frequency Control* 51 (11) (2004) 1547–1556, http://dx.doi.org/10.1109/TUFFC.2004.1367496.
[33] W. Luo, J.L. Rose, Phased array focusing with guided waves in a viscoelastic coated hollow cylinder, *Journal of the Acoustical Society of America* 121 (4) (2007) 1945–1955, http://dx.doi.org/10.1121/1.2711145.
[34] J. Mu, J.L. Rose, Guided wave propagation and mode differentiation in hollow cylinders with viscoelastic coatings, *Journal of the Acoustical Society of America* 124 (2) (2008) 866–874, http://dx.doi.org/10.1121/1.2940586.
[35] J. Hua, J. Mu, J.L. Rose, Guided wave propagation in single and double layer hollow cylinders embedded in infinite media, *Journal of the Acoustical Society of America* 129 (2) (2011) 691–700, http://dx.doi.org/10.1121/1.3531807.
[36] J. Hua, J. Mu, J.L. Rose, Guided wave propagation and focusing in multi-layer pipe with viscoelastic coating and infinite soil media, *Materials Evaluation*0025-532771 (3) (2013) 369–377.
[37] H. Kwun, S.Y. Kim, M.S. Choi, S.M. Walker, Torsional guided-wave attenuation in coal-tar-enamel-coated, buried piping, *NDT & E International* 37 (2004) 663–665, http://dx.doi.org/10.1016/j.ndteint.2004.05.003.
[38] R. Kirby, Z. Zlatev, P. Mudge, On the scattering of torsional elastic waves from axisymmetric defects in coated pipes, *Journal of Sound and Vibration* 331 (17) (2012) 3989–4004, http://dx.doi.org/10.1016/j.jsv.2012.04.013.
[39] R. Kirby, Z. Zlatev, P. Mudge, On the scattering of longitudinal elastic waves from axisymmetric defects in coated pipes, *Journal of Sound and Vibration* 332 (20) (2013) 5040–5058, http://dx.doi.org/10.1016/j.jsv.2013.04.039.
[40] H.V. Fuchs, R. Riehle, Ten years of experience with leak detection by acoustic signal analysis, *Applied Acoustics* 33 (1) (1991) 1–19, http://dx.doi.org/10.1016/0003-682X(91)90062-J.

[41] J.M. Muggleton, M.J. Brennan, R.J. Pinnington, Wavenumber prediction of waves in buried pipes for water leak detection, *Journal of Sound and Vibration* 249 (5) (2002) 939–954, http://dx.doi.org/10.1006/jsvi.2001.3881.
[42] R. Long, P. Cawley, M.J.S. Lowe, Acoustic wave propagation in buried iron pipes, *Proceedings of the Royal Society of London: Series A* 459 (2003) 2749–2770, http://dx.doi.org/10.1098/rspa.2003.1148.
[43] W.T. Thomson, Transmission of elastic waves through a stratified solid medium, *Journal of Applied Physics* 21 (1950) 89–93, http://dx.doi.org/10.1063/1.1699629.
[44] N.A. Haskell, The dispersion of surface waves on multilayered media, *Bulletin of the Seismological Society of America* 43 (1) (1953) 17–34. ISSN 0037-1106.
[45] L. Knopoff, A matrix method for elastic wave problems, *Bulletin of the Seismological Society of America*0037-110654 (1) (1964) 431–438.
[46] M.J.S. Lowe, Matrix techniques for modelling ultrasonic waves in multi-layered media, *IEEE Transactions on Ultrasonics Ferroelectrics and Frequency Control* 42 (4) (1995) 525–542, http://dx.doi.org/10.1109/58.393096.
[47] B. Pavlakovic, M.J.S. Lowe, D. Alleyne, P. Cawley, Disperse: a general purpose program for creating dispersion curves, D.O. Thompson, D.E. Chimenti (Eds.), *Review of Progress in Quantitative Nondestructive Evaluation*, Vol. 16A, Springer, New York1997, pp. 185–192, http://dx.doi.org/10.1007/978-1-4615-5947-4_24.
[48] B. Pavlakovic, M.J.S. Lowe, A general purpose approach to calculating the longitudinal and flexural modes of multi-layered, embedded, transversely isotropic cylinders, D.O. Thompson, D.E. Chimenti (Eds.), *Review of Progress in Quantitative Nondestructive Evaluation*, Vol. 18 A, Springer, New York1999, pp. 239–246, http://dx.doi.org/10.1007/978-1-4615-4791-4_29.
[49] J.C. Santamarina, K.A. Klein, M.A. Fam, *Soils and Waves*, Wiley, Chichester. ISBN: 0-471-49058-X, 2001.
[50] K.H. Stokoe II, R.D. Woods, in situ shear wave velocity by cross-hole method, *Journal of the Soil Mechanics and Foundations Division* 98 (5) (1972) 443–460. ISSN 0044-7994.
[51] R. Bachrach, J. Dvorkin, A.M. Nur, Seismic velocities and Poisson's ratio of shallow unconsolidated sands, *Geophysics* 65 (2) (2000) 559–564, http://dx.doi.org/10.1190/1.1444751.
[52] R. Bachrach, M. Reshef, 3D ultra shallow seismic imaging of buried pipe using dense receiver array: practical and theoretical considerations, *Geophysics* 75 (6) (2010) G41–G51, http://dx.doi.org/10.1190/1.3506560.
[53] W.L. Nyborg, I. Rudnick, H.K. Schilling, Experiments on acoustic absorption in sand and soil, *Journal of the Acoustical Society of America* 22 (4) (1950) 422–425, http://dx.doi.org/10.1121/1.1906620.
[54] W. Brutsaert, J.N. Luthin, The velocity of sound in soils near the surface as a function of the moisture content, *Journal of Geophysical Research* 69 (4) (1964) 643–652, http://dx.doi.org/10.1029/JZ069i004p00643.
[55] R.m. Koerner, A.E. Lord Jr., W.M. McCabe, J.W. Curran, Acoustic emission of granular soils, *Journal of Geotechnical Engineering Division*0093-6405102 (7) (1976) 761–773.
[56] D. Velea, F.D. Shields, J.M. Sabatier, Elastic wave velocities in partially saturated Ottawa sand: experimental results and modelling, *Soil Science Society of America* 64 (2000) 1226–1234, http://dx.doi.org/10.2136/sssaj2000.6441226x.
[57] M.L. Oelze, W.D. O'Brien Jr., R.G. Darmody, Measurement of attenuation and speed of sound in soils, *Soil Science Society of America* 66 (2002) 788–796, http://dx.doi.org/10.2136/sssaj2002.7880.
[58] M. Kimura, Shear wave speed dispersion and attenuation in granular marine sediments, *Journal of the Acoustical Society of America* 134 (1) (2013) 144–155, http://dx.doi.org/10.1121/1.4809679.
[59] M. Kimura, Grain-size dependence of shear wave speed dispersion and attenuation in granular marine sediments, *Journal of the Acoustical Society of America* 136 (1) (2014) EL53–EL59, http://dx.doi.org/10.1121/1.4885478.
[60] P.K. Robertson, S. Sasitharan, J.C. Cunning, D.C. Sego, Shear-wave velocity to evaluate in-situ state of Ottawa sand, *Journal of Geotechnical Engineering* 121 (3) (1995) 263–273, http://dx.doi.org/10.1061/(ASCE)0733-9410(1995)121:3(262)).
[61] M. Fam, J.C. Santamarina, A study of consolidation using mechanical and electromagnetic waves, *Géotechnique* 47 (2) (1997) 203–219, http://dx.doi.org/10.1680/geot.1997.47.2.203.
[62] J.S. Lee, J.C. Santamarina, Bender elements: performance and signal interpretation, *Journal of Geotechnical and Geoenvironmental Engineering* 131 (9) (2005) 1063–1070, http://dx.doi.org/10.1061/(ASCE)1090-0241(2005)131:9(1063).
[63] B.O. Hardin, J. Music, Apparatus for vibration of soil specimens during a triaxial test, *Instruments and Apparatus for Soil and Rock Mechanics, American Society for Testing and Materials, ASTM STP* 392 (STP41278S) (1965) 55–74, http://dx.doi.org/10.1520/STP41278S.
[64] G. Gazetas, K.H. Stokoe II, Free vibration of embedded foundations: theory versus experiment, *Journal of Geotechnical Engineering* 117 (9) (1991) 1382–1401, http://dx.doi.org/10.1061/(ASCE)0733-9410(1991)117:9(1382).
[65] D. Fratta, J.C. Santamarina, Wave propagation in soils: multi-mode, wide-band testing in a waveguide device, *Geotechnical Testing Journal* 19 (2) (1996) 130–140, http://dx.doi.org/10.1520/GTJ10336J.
[66] M. Prasad, R. Meissner, Attenuation mechanisms in sands: laboratory versus theoretical (Biot) data, *Geophysics* 57 (5) (1992) 710–719, http://dx.doi.org/10.1190/1.1443284.
[67] M. Prasad, Acoustic measurements in unconsolidated sands at low effective pressure and overpressure detection, *Geophysics* 67 (2) (2002) 405–412, http://dx.doi.org/10.1190/1.1468600.
[68] M.A. Zimmer, M. Prasad, G. Mavko, A. Nur, Seismic velocities of unconsolidated sands: part 1 – pressure trends from 0.1 to 20 MPa, *Geophysics* 72 (1) (2007) E1–E13, http://dx.doi.org/10.1190/1.2399459.
[69] ASTM D2487. 2011 Standard practice for classification of soils for engineering purposes (unified soil classification system). Annual Book of ASTM Standards. Vol. 04.08. ASTM Intlernational (http://dx.doi.org/10.1520/D2487-11).
[70] A. Galvagni, P. Cawley, The reflection of guided waves from simple supports in pipes, *Journal of the Acoustical Society of America* 129 (4) (2001) 1869–1880, http://dx.doi.org/10.1121/1.3543958.
[71] E. Leinov, P. Cawley, M.J.S. Lowe, Investigation of guided waves propagation in pipe buried in sand AIP Conference Proceeding, Vol. 1581, D.E. Chimenti, L.J. Bond, D.O. Thompson (Eds.), *Proceedings of the 40th Annual Review of Progress in Quantitative Nondestructive Evaluation*, Vol. 33A, AIP, New York, 2014, pp. 271–278, http://dx.doi.org/10.1063/1.4864830.
[72] Y.-S. Fang, Y.-C. Ho, T.-J. Chen, Passive earth pressure with critical state concept, *Journal of Geotechnical and Geoenvironmental Engineering* 128 (2002) 651–659, http://dx.doi.org/10.1061/(ASCE)1090-0241(2002)128:8(651).
[73] T.-J. Chen, Y.-S. Fang, Earth pressure due to vibratory compaction, *Journal of Geotechnical and Geoenvironmental Engineering* 134 (2008) 437–444, http://dx.doi.org/10.1061/(ASCE)1090-0241(2008)134:4(437).
[74] T. Vogt, M. Lowe, P. Cawley, Cure monitoring using ultrasonic guided waves in wires, *Journal of the Acoustical Society of America* 114 (3) (2003) 1303–1313, http://dx.doi.org/10.1121/1.1589751.